UNCLASSIFIED

SECURITY CLASSIFICATION OF THIS PAGE (When Data Entered)

AD-A197 222

REPORT DOCUMENTATION PAGE	READ INSTRUCTIONS BEFORE COMPLETING FORM
1. REPORT NUMBER: AFIT/CI/NR 88-177	2. GOVT ACCESSION NO.
3. RECIPIENT'S CATALOG NUMBER: DTIC FILE COPY	
4. TITLE (and Subtitle) ENERGY DEPENDENCE OF THE QUENCHING CROSS SECTION FOR THE REACTION OF METASTABLE ARGON AND WATER	5. TYPE OF REPORT & PERIOD COVERED: MS THESIS
	6. PERFORMING ORG. REPORT NUMBER
7. AUTHOR(s): STEPHEN WAYNE NOVICKI	8. CONTRACT OR GRANT NUMBER(s)
9. PERFORMING ORGANIZATION NAME AND ADDRESS: AFIT STUDENT AT: RUTGERS UNIVERSITY	10. PROGRAM ELEMENT, PROJECT, TASK AREA & WORK UNIT NUMBERS
11. CONTROLLING OFFICE NAME AND ADDRESS	12. REPORT DATE: 1988
	13. NUMBER OF PAGES: 57
14. MONITORING AGENCY NAME & ADDRESS (if different from Controlling Office): AFIT/NR, Wright-Patterson AFB OH 45433-6583	15. SECURITY CLASS. (of this report): UNCLASSIFIED
	15a. DECLASSIFICATION/DOWNGRADING SCHEDULE

16. DISTRIBUTION STATEMENT (of this Report)

DISTRIBUTED UNLIMITED: APPROVED FOR PUBLIC RELEASE

17. DISTRIBUTION STATEMENT (of the abstract entered in Block 20, if different from Report)

SAME AS REPORT

18. SUPPLEMENTARY NOTES

Approved for Public Release: IAW AFR 190-1
LYNN E. WOLAVER 8 Aug 88
Dean for Research and Professional Development
Air Force Institute of Technology
Wright-Patterson AFB OH 45433-6583

19. KEY WORDS (Continue on reverse side if necessary and identify by block number)

20. ABSTRACT (Continue on reverse side if necessary and identify by block number)

ATTACHED

DTIC ELECTE AUG 17 1988 S D H

DD FORM 1 JAN 73 1473 EDITION OF 1 NOV 65 IS OBSOLETE

UNCLASSIFIED

SECURITY CLASSIFICATION OF THIS PAGE (When Data Entered)

88 8 16 01

ENERGY DEPENDENCE OF THE QUENCHING CROSS SECTION FOR THE REACTION OF METASTABLE ARGON AND WATER

By STEPHEN WAYNE NOVICKI

A thesis submitted to the

Graduate School-New Brunswick

Rutgers, The State University of New Jersey

in partial fulfillment of the requirements

for the degree of

Master of Science

Graduate Program in Chemistry

Written under the direction of

Professor John Krenos

and approved by

John Krenos

New Brunswick, New Jersey

October 1987

ABSTRACT OF THE THESIS

Energy Dependence of the Quenching Cross Section for the Reaction of Metastable Argon and Water

by STEPHEN WAYNE NOVICKI

Thesis Director: Professor John Krenos

This work examines the energy dependence of the quenching cross section (σ_Q) for the reaction of metastable argon ($Ar(^3P_{2,0})$) with ground state water ($H_2O(^1A_1)$). A molecular beam and scattering gas apparatus is employed. The energy dependence of the quenching cross section is determined by observing the intensity of the fluorescence from the reaction product $OH(A^2\Sigma^+ \rightarrow X^2\Pi_i)$ vs. the scattering gas pressure for a series of metastable beam energies. The method for determining the quenching cross section was adapted from a 1975 paper by Dickson and Zare, and is the first time this procedure has been used to measure the energy dependence of the quenching of metastable species by ground state molecules. The uncorrected quenching cross section and the deconvoluted cross section were determined to vary with energy as $E^{-0.83}$ and $E^{-0.50}$, respectively. The quenching process for this system was determined to be governed by long range attractive forces.

QUALITY INSPECTED 2

For
I
Unannounced
Justification
By
Distribution/
Availability Codes
Dist | Avail and/or Special
A-1

TABLE OF CONTENTS

LIST OF TABLES

LIST OF FIGURES

CHAPTER I. INTRODUCTION

A. BACKGROUND

In order to understand the physical world, we must investigate the basic forces which cause our world to change. In chemistry, it is important to investigate the interactions of species on the molecular level in order to understand and predict reaction processes. Experimental methods such as flowing afterglow, pulsed radiolysis, shock tubes, flash photolysis and molecular beams[1-2] are used to investigate the dynamics of chemical processes.

Molecular beam techniques make it possible to study the properties associated with single collision encounters between molecules, such as product velocity distributions. In typical molecular beam experiments, these distributions are not resolved sufficiently to determine product rotational or vibrational distributions. The combination of molecular beam and spectroscopic techniques has allowed the detailed determination of product internal energy distributions. Thus, it is possible to determine the electronic, vibrational and rotational distributions of product molecules produced by well-defined collisions.

The scope of this project was to examine the chemical dynamics of electronically excited metastable atoms reacting with ground state molecules to form electronically excited neutral products. In many reactions of this type, it has been possible to determine the reaction cross

section for the formation of the excited products, which are in specific electronic and vibrational states, as a function of the collision energy. The study of this type of reaction is of great practical interest due to its importance in atmospheric and laser chemistry.

Rare gas metastables have been used to produce suitable population inversions for lasing in systems such as He-Ne, Ar-O_2 and Ar-N_2. In the case of He-Ne, the energy transfer process which produces lasing is:

$$He(2^3S) + Ne(1^1S_0) \text{ ------> } He(1^1S_0) + Ne(2s) \qquad (1)$$

where metastable helium is quenched by neon, producing an electronically excited neon atom which can decay to the 2p state, giving off a lasing photon. The 2s and 2p symbols define the $2p^5 4s$ and $2p^5 3p$ configurations of neon, respectively.[3]

An example of how this class of reactions might affect the upper atmosphere, is the reaction of excited nitrogen molecules (produced by optical pumping or electron impact) with oxygen molecules to form N_2O. This process could augment considerably the biogenic source of N_2O on the surface of the Earth.[4]

Metastable atoms are electronically excited species with "exceptionally" long lifetimes. The minimum lifetime for an electronically excited metastable species is approximately 1 μsec, which implies that electronic dipole radiative transitions must be forbidden for a species to be

in the metastable state.[5]

The long lifetimes of metastable atoms make them attractive in the study of reaction dynamics since they can be isolated from short lived excited species and their reactions studied. Of special interest are metastable rare gas atoms since they have extremely long lifetimes and are very energetic and reactive.

The metastable atom of interest in this work is $Ar(^3P_{2,0})$. These excited states of argon are the result of the excitation of an electron from the 3p to the 4s orbital. This results in excitation energies of 11.55 and 11.72 eV and calculated lifetimes of 56 and 45 seconds for the $^3P_2$ and $^3P_0$ states, respectively.[6]

The interaction of Ar^* with ground state H_2O has been examined in previous work and is the subject of this paper. A major reaction pathway in this system was shown to be:

$$Ar(^3P_{2,0}) + H_2O(^1A_1) \rightarrow Ar(^1S_0) + OH(A^2\Sigma^+) + H(^2S) \quad (2)$$

This reaction is believed to account for much of the quenching cross section of metastable argon and water. Following this reaction, the electronically excited $OH(A^2\Sigma^+)$ undergoes an electronic transition from $A^2\Sigma^+ \rightarrow X^2\Pi$, with an emission in the 2800 to 3400 A region. The precise mechanism for the electronic energy transfer (quenching), followed by the dissociation of water is not yet clear. Probable mechanisms have been proposed by Clyne et al.[7] and Snyder et al.[8]

B. SCOPE OF PRESENT WORK

In order to understand the quenching process, information on the total quenching cross section as a function of collision energy, $\sigma_0(E)$, is required. Previous studies have determined values for $\sigma_0(E)$, however, these values vary widely. For example, Sheldon and Muschlitz[9] reported that the total quenching cross section of $Ar(^3P_{2,0})$ was independent of energy, while Parr and Martin[10] and Corn[11] reported that the cross section for reaction (2) varies as $E^{-0.34}$ and $E^{-0.60}$, respectively.

The differences in the results obtained for the energy dependence of the cross section can be attributed, in part, to the methods used to obtain the data. In the case of Sheldon and Muschlitz,[9] a beam and scattering cell system was used. The metastable beam intensities were measured by the electron current produced by an Auger process at the gold plated walls of the scattering cell. A simple Beer-Lambert relation describes the change in the quenching cross section of the reaction as the scattering gas pressure is increased,

$$\sigma_0 = \frac{\ln (I^0 / I)}{n_{SG}\, l} \qquad (3)$$

here I^0 is the electron current seen without scattering gas in the cell, I is the electron current when the scattering gas number density is n_{SG} and l is the scattering cell length.[9] The method used in this experiment to measure the

intensity of the metastable beam can be unreliable in the case where long lived excited products with enough energy to eject electrons from the scattering cell walls are present, or if contaminants (such as scattering gas) have been adsorbed onto the wall of the cell.[9]

In this work, the problems which might have affected the results of the above mentioned work are avoided. Since the quenching of Ar^* by H_2O produces a product which emits light, the light intensity I^*, can be recorded at a given distance, x, from the entrance of the scattering cell as a function of the scattering gas number density, n_{sG}. This allows the calculation of $\sigma_Q(E)$ from

$$I^* \propto \sigma^* \; v \; n_{sG} \; n^0{}_{m^*} \; \exp(-\sigma_Q \; n_{sG} \; x) \qquad (4)$$

where

$$n^0{}_{m^*} \ll n_{sG} \qquad (5)$$

and σ^* is the cross section for the light producing channel (in this case OH ($A^2\Sigma^+ \rightarrow X^2\Pi_i$)), v is the relative velocity of the species, and $n^0{}_{m^*}$ is the metastable atom number density without scattering gas present.

In order to find σ_Q, the maximum of equation 4 must be found. At the maximum, $dI^*/dn_{sG} = 0$ from which we obtain

$$\sigma_Q = \frac{1}{n_{sG} \; x} \qquad (6)$$

The scattering gas number density being defined as:

$$n_{sG} = \frac{NP}{RT} \qquad (7)$$

where N is Avogadro's constant, R is the gas constant, P is

the scattering gas pressure and T is the scattering gas temperature. In this study, the metastable beam energy is varied in order to determine $\sigma_Q(E)$.[12] This method of measuring σ for chemiluminescent reactions was described by Dickson and Zare[13] in a study of the relative chemiluminescent intensity as a function of oxidant pressure for the reaction of Sm with O_3, N_2O and NO_2. Our study is the first time their method has been used for studying the energy dependence of σ_0.

CHAPTER II. APPARATUS

A. GENERAL DESCRIPTION

The molecular beam apparatus used in this investigation is shown schematically in Figure 1. A brief description of this system will be given in this section, with a more detailed description of the individual components following.

The instrument consists of three differentially pumped sections or chambers; the nozzle chamber, the buffer chamber and the main or reaction chamber. The beam gas enters the system through the nozzle chamber, where it undergoes a supersonic expansion through an adjustable temperature, pinhole nozzle. The gas exiting the nozzle passes through a skimmer and enters the buffer chamber. In this chamber, the beam gas is bombarded with electrons in order to produce a small fraction of excited gas atoms. Charged particles and Rydberg states in the beam are quenched by an electrostatic field at the exit of the chamber. The main chamber contains the scattering or reaction cell which is maintained at room temperature. This cell is located far enough downstream from the entrance of the chamber so that short lived excited atoms ($\tau < 120\mu sec$), can radiate prior to entering the collision/reaction region. The beam gas entering the scattering cell is therefore composed of ground-state and metastable species. The intensity of the metastable beam

FIGURE 1. Schematic diagram of the molecular beam reaction system.

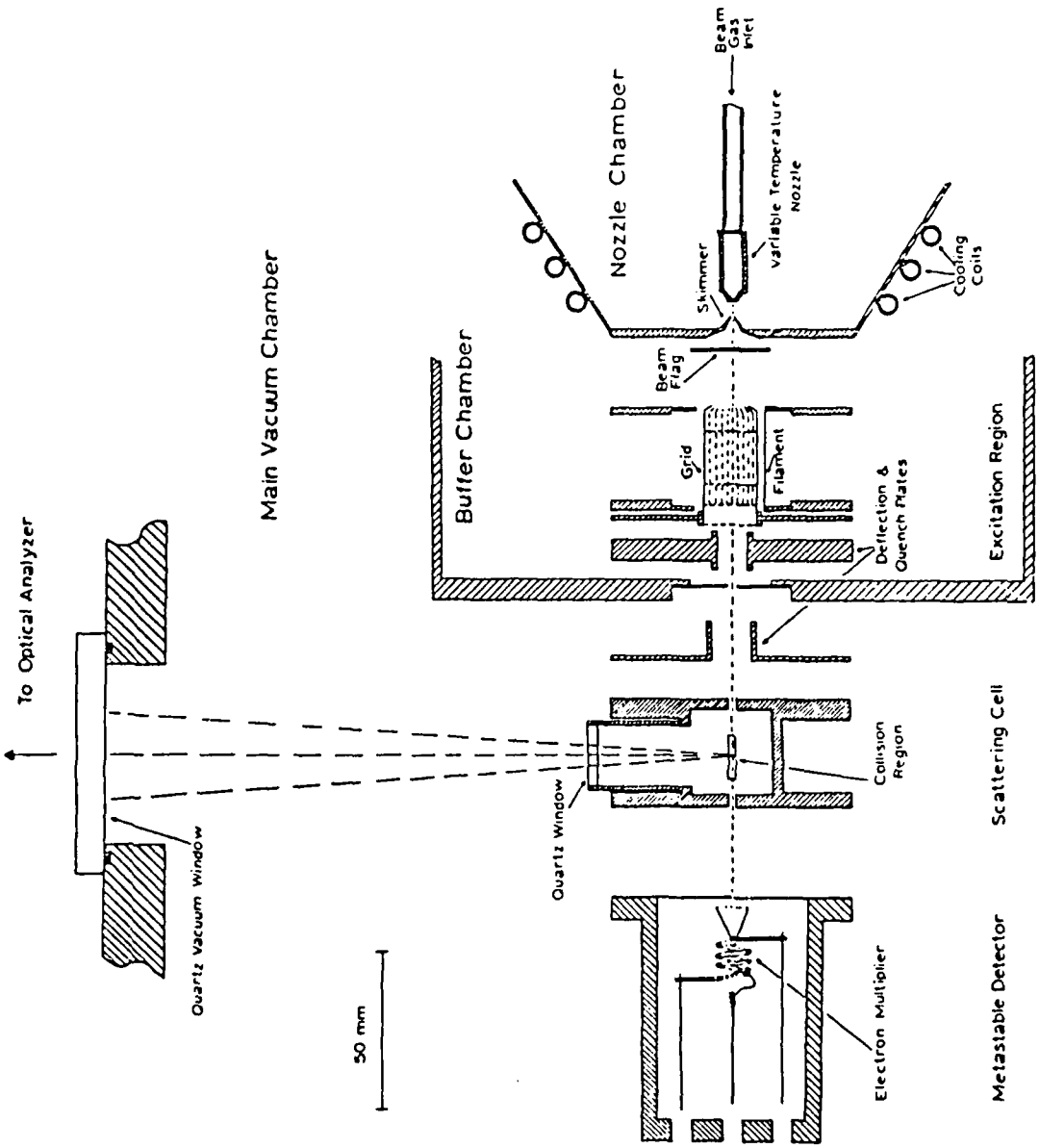
To Optical Analyzer
Main Vacuum Chamber
Buffer Chamber
Nozzle Chamber
Beam Gas Inlet
Variable Temperature Nozzle
Skimmer
Cooling Coils
Beam Flag
Grid
Filament
Deflection & Quench Plates
Excitation Region
Quartz Vacuum Window
Quartz Window
Collision Region
Scattering Cell
50 mm
Electron Multiplier
Metastable Detector

was monitored by a particle multiplier at the exit of the scattering cell.

The light emission from the reaction of the metastable beam and the scattering gas was collected through quartz windows mounted normal to the beam path in the walls of the scattering cell and main chamber. This light was focused onto the entrance slit of a scanning monochromator with a cooled photomultiplier tube attached to the exit slit. The intensity of the light was measured using a single-photon counting system.

B. DETAILED DESCRIPTION

1. REACTANT GAS DELIVERY

Figures 2 and 3 show the manifold systems used to control the beam and scattering gases, respectively.

Prior to conducting an experiment, both manifolds were evacuated to a pressure of 20 μm, by a mechanical pump. Beam gas was obtained from commercially supplied bottled gas (Matheson). This gas was regulated to an outlet pressure of 15 psig and fed into the beam gas distribution system. The gas passed through a particulate filter, a shutoff valve (1), and through a needle valve (3). The needle valve was used, in conjunction with an absolute pressure gauge, to adjust the beam gas back pressure. If higher beam gas energies were required, the beam gas could be seeded with a lighter nonreacting gas, by passing the seed gas through a similar filter and valving system as

FIGURES 2 AND 3. Inlet manifold diagrams for beam gas and scattering gas.

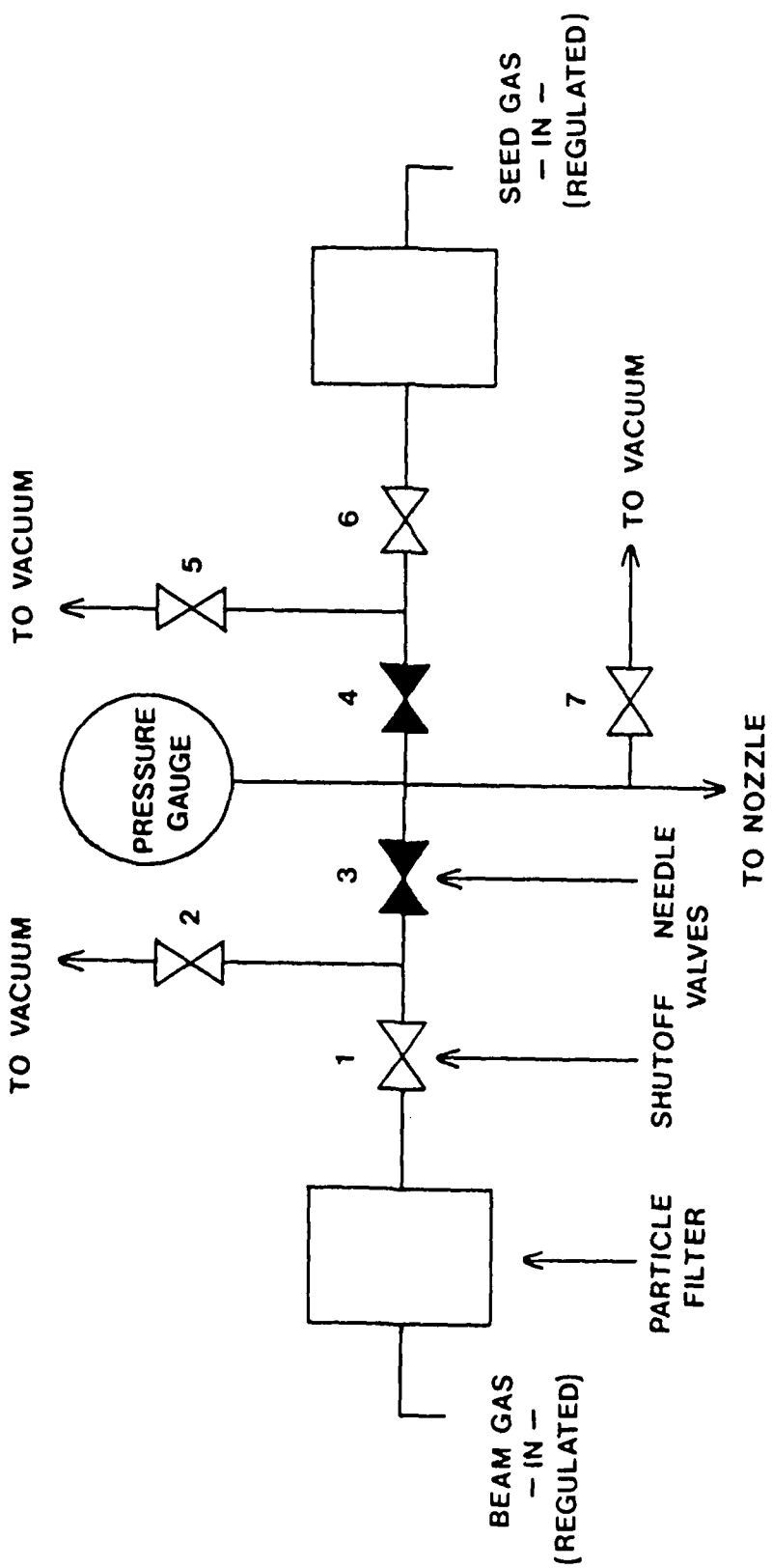
SEED GAS
– IN –
(REGULATED)
TO VACUUM
TO VACUUM
TO VACUUM
PRESSURE
GAUGE
1
2
3
4
5
6
7
SHUTOFF NEEDLE
VALVES
TO NOZZLE
PARTICLE
FILTER
BEAM GAS
– IN –
(REGULATED)

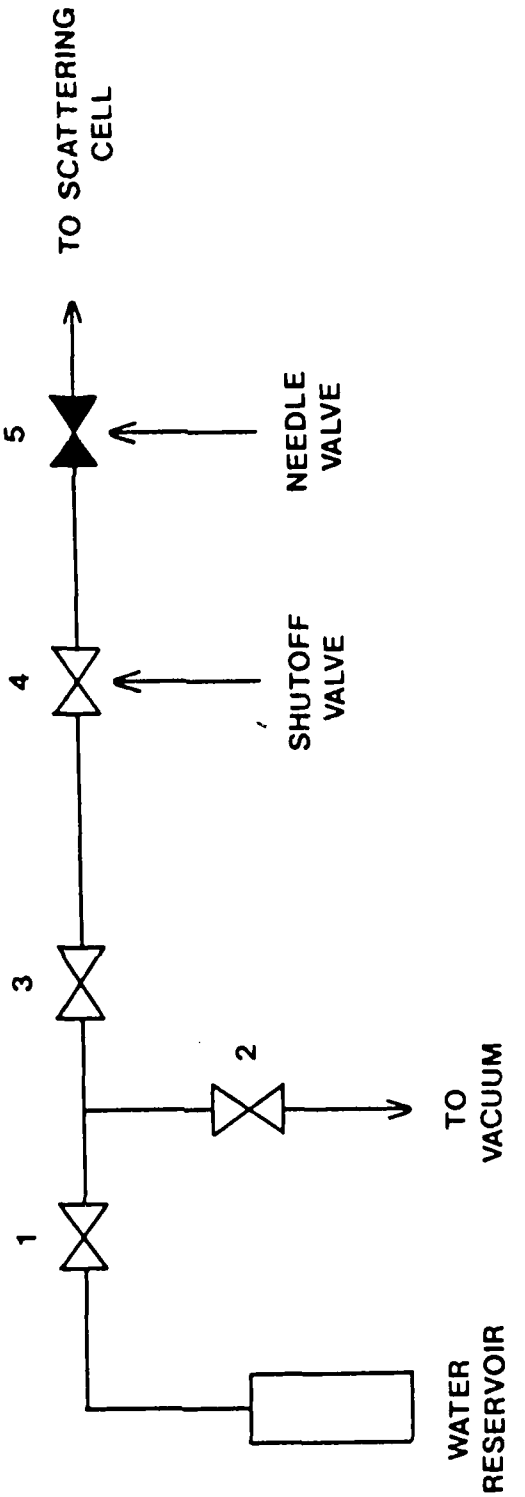
TO SCATTERING CELL
NEEDLE VALVE
SHUTOFF VALVE
TO VACUUM
WATER RESERVOIR
1
2
3
4
5

that used for the beam gas.

The scattering gas, which in this case was H_2O and D_2O (Cambridge Isotope Lab, 99.96% D) vapor, was generated by placing a small amount (about 10 ml) of the appropriate liquid in the scattering gas reservoir. This reservoir was evacuated until a pressure of approximately 30 μm was obtained. This insured that dissolved gases, especially nitrogen, were removed from the liquid. The vapor which formed above the liquid in the reservoir was then allowed to effuse into the scattering cell. The amount of scattering gas which was allowed to flow into the scattering cell was controlled by a needle valve (5).

2. BEAM GENERATION

The molecular beam used for this experiment was generated by expanding the beam gas through a pinhole nozzle (aperture 130 μm in diameter) in order to generate a supersonic beam. This beam passed through a skimmer (aperture 1mm in diameter) located 7 mm downstream from the nozzle. The design of the nozzle and the skimmer are taken from Lee and Herschbach,[14] and Bier and Hagena,[15] respectively. The nozzle was surrounded by a series of tantalum wire heating elements, which allowed the nozzle temperature to be varied between 295 and 950 K. The nozzle temperature was measured by the use of a chromel-alumel thermocouple attached to the nozzle/heating element.

The collimated supersonic beam which emerges from the

skimmer, passes into the excitation region of the buffer chamber. In this region, electrons ejected from a hot, 2% thoriated-tungsten, filament collide with a small fraction of the beam gas atoms, in order to produce an excited species. The electrons ejected from the tungsten filament were accelerated into the beam path by a platinum coated cylindrical molybdenum grid, through which the supersonic beam passed coaxially.

The filament temperature was regulated by a current-regulated power supply. In order to obtain filament temperatures above 2000 K, a current of approximately 5 amps was employed.[11]

The potential placed on the grid was applied in various ways, depending on the experimental applications. During data runs designed to gather information an collision cross sections at low to moderate beam energies, the grid potential was set at a potential between 80 and 150 V, which maximized the beam signal, the specific potential being a function of the age of the tungsten filament.

In order to determine the approximate beam energies for seeded beams, a time-of-flight analysis was used. This required that the potential to the grid be pulsed rather than continuous. A discussion of the circuitry used for this process can be found in Bel Bruno.[16]

The collisional excitation of the beam gas generated

some rare gas ions and Rydberg state atoms, which if not removed from the beam might interfere with the collection of data. Removal of these species, as well as electrons which may have been accelerated by the grid in the direction of the beam, was accomplished by a set of deflection and quenching plates, located downstream from the grid. The deflection/quenching plates consisted of two semicircular, stainless steel plates, positioned approximately 1 cm apart. One plate was maintained at approximately -630 VDC by a set of storage cells, the remaining plate was grounded. This potential was sufficient to quench Rydberg states and deflect any charged particles.

3. VACUUM SYSTEM

As mentioned earlier, the apparatus consisted of three differentially pumped chambers. The first chamber being the nozzle chamber. This section was evacuated to approximately 1 X 10^{-6} torr by a 16 inch oil diffusion pump, which was backed by a large capacity mechanical pump (Stokes Micro Vac., model 212H-10). The foreline pressure was monitored by a thermocouple gauge. The requirement for such large pumping is dictated by the relatively large amount of gas which had to be removed due to the skimming of the beam gas.

The second, or buffer chamber, was pumped down to approximately 1 X 10^{-6} torr by a six inch oil diffusion

pump, which was backed by a mechanical pump (Welch model 1374). The pressure in this chamber being monitored by an ionization gauge.

The third or main chamber was evacuated to approximately 1.2 X 10^{-6} torr by a six inch oil diffusion pump and was backed by a mechanical pump (Welch model 1397). The chamber pressure was monitored by means of an ionization gauge.

During the course of experimentation, several vacuum system related problems were encountered, which required the installation of additional equipment. Two diffusion pumps (Buffer and Main Chamber) were mated to their respective chambers with water cooled aluminum baffles sandwiched in between. At the start of this project, the water cooling feature of these baffles was not used. This was due to the unusually short time before the aluminum tubes became corroded and blocked, rendering the water cooling feature of the baffles useless. As experimentation progressed, a fine oil mist began to form on the walls of the main chamber and ultimately on the quartz viewing window. This caused the observed intensity of the light from the reaction to decrease drastically. In order to partially correct this problem, two changes were made to the main chamber vacuum system. A piece of 1/4 inch copper tubing was wrapped around the outside of the main chamber baffle plate and connected to the photomultiplier cooling

system, downstream of the photomultiplier. In addition to this change, a molecular sieve baffle (Lester, MMA-150) was installed in the line between the mechanical and oil diffusion pumps to prevent the possible migration of mechanical pump fluid from contaminating the diffusion pump oil, thus allowing it to vaporize and migrate into the main chamber.

4. MAIN CHAMBER

The main chamber contained the scattering (reaction) cell. The scattering cell temperature was maintained at room temperature throughout the experiments and was located 94 mm down stream from the beam excitation region, which allows short lived species (τ < 120 μsec) to radiate prior to reaching the scattering cell. Thus, the beam entering the scattering cell consisted of ground state Ar atoms and $Ar(^3P_{2,0})$ metastables. The cell has a cylindrical shape, with a total path length of 35.3 mm from entrance to exit openings. The internal path length is approximately 26 mm. The entrance aperture is approximately 1.6 mm in diameter, the exit aperture is 2.4 mm. The scattering gas pressure in the cell was monitored by a capacitance manometer (MKS, model 227 AHS) with digital read out.

Light resulting from the reaction of the metastable beam and the scattering gas was observed normal to the beam path through a quartz window in the side of the cell. This light then passed through a 3 inch diameter quartz window

in the main chamber. A light tunnel arrangement was used between the scattering cell window and the main chamber viewing window to prevent vacuum pump oil vapor from condensing on the scattering cell window. In addition, a heated brass tube was attached to the mounting plate of the 3 inch quartz window. This tube served two purposes, that of a light shield and as a heat sink to warm the quartz window and prevent vacuum pump oil from condensing on it.

The metastable beam intensity was measured at the exit of the scattering cell. This measurement was made in order to determine the stability of the metastable beam during the course of the experiment, and was not required to determine the reaction cross section. The beam intensity was also used to measure the arrival time of the metastable atoms during the time of flight experiments. Depending on the application, different detectors were installed in the system. They were located approximately 45 mm from the scattering cell exit, the exact position being a function of the particular detector. During test runs without a seeded beam, the particle multiplier consisted of a piece of tungsten foil maintained at a potential difference of -1200 VDC from the wall of the metastable detector. Time-of-flight measurements required the use of a Galileo continuous channel electron multiplier (channeltron), operated at voltages ranging between -2100 and -2600 VDC (with a -300 VDC bias voltage). The output from either

system was fed into a current amplifier and monitored by a digital multimeter in the case of an unseeded beam and by a oscilloscope in the case of a seeded beam.

The time-of-flight experiments required that the metastable beam be pulsed. This could have been accomplished by a mechanical chopper mechanism, but it was simpler to pulse the voltage to the electron acceleration grid in order to generate pulsed metastables. The voltage pulses were generated via a pulse generator described in Bel Bruno.[16] The output from this system was monitored on an oscilloscope, which superimposed the current pulse to the high voltage pulse generator and the metastable beam intensity signal from the channeltron detector.

5. OPTICAL SYSTEM

The light which exited the main chamber quartz window was focused, by a bi-convex lens, onto the entrance slit of a 0.5 meter, f/6.9 Spex monochromator (model 870). The monochromator was mounted on end, so that the micrometer slit-width adjustment controlled the width (vertical) of the light from the scattering cell and the slit height adjuster regulated the length (horizontal) of the observation region. The settings used for this series of experiments were 3 mm for the micrometer setting and the length of the region was 2 mm. A 1200 grove/mm grating, blazed at 3000 A was used in the monochromator. The monochromator was adjusted so that light of wavelength

3101.7 A was passed through the exit slits (set at 3mm aperture, bandpass 48 A) and focussed onto a cooled photomultiplier tube (RCA 31034). A single photon counting system (PAR model 1110) was used to record the intensity of the light given off during the scattering event. The wavelength of 3101.7 A corresponds to a low resolution peak in the OH ($A^2\Sigma \rightarrow X^2\Pi_1$) spectrum, determined in previous work.[16]

III. EXPERIMENTAL PROCEDURE

A. GENERAL PROCEDURE

Several pieces of equipment were operated continuously in order to maintain stable conditions for data gathering. This equipment included such things as the diffusion and mechanical vacuum pumps, the photomultiplier tube power and cooling system, the capacitance manometer and the current to the heater of the main chamber optical window.

There were many situations which required maintenance of the system. If this maintenance required access to any of the evacuated chambers, the diffusion pumps would have to be shut down (isolation of the mechanical pumps from the system made it unnecessary to shut these units down) and the chambers were vented to the atmosphere. Once maintenance was completed, the system was allowed to evacuate overnight to insure that suitable operating pressures were achieved prior to taking data.

The item which required the most maintenance in this apparatus was the thoriated-tungsten filament used to generate metastable atoms. Momentary power interruptions were usually sufficient to cause the filament to break due to thermal shock. In addition, as the filament aged, it began to expand and eventually came into contact with the electron acceleration grid, causing a short which required replacement of the filament. After replacing the filament, a period spanning one to four days was required to allow

the filament to "condition."

Prior to conducting a data run, the metastable beam gas delivery manifold and the scattering gas manifold were evacuated to remove contaminant gases, such as nitrogen, which might interfere with the experiment. In addition, power to the photon counting system was turned on at this time.

Once the system was evacuated, power was provided to the metastable detector, the electron acceleration grid and the deflection and quenching plates. A metastable beam was generated by allowing beam gas to enter the beam gas manifold. When the nozzle back pressure reached the desired value, the beam was unflagged and the intensity of the metastable beam and the nozzle temperature were recorded. At this time, the capacitance manometer which measured the scattering cell pressure was zeroed. Following this, the beam was flagged, the scattering gas was introduced into the scattering cell and the pressure allowed to stabilize at .2 ± .05 millitorr. During the time required for the scattering gas pressure to stabilize, the room lights were extinguished and the background photon count was measured. In addition, the room temperature was recorded. Once the scattering gas pressure stabilized, the beam was unflagged and the photon counter was started. The counter was allowed to count for one minute and the intensity of the fluorescence was recorded. The scattering

gas pressure was increased by an additional .2 millitorr and the pressure in the cell was allowed to stabilize for a minimum of two minutes. The intensity of fluorescence from the scattering cell was measured and recorded. This procedure was continued until a peak in the intensity of the observed fluorescence was encountered or until the scattering cell pressure could not be increased. Once a peak was observed, the pressure interval between photon counting was increased from .2 to .3 millitorr, and measurements were taken until the scattering cell pressure could not be increased. When the maximum scattering cell pressure was reached, the scattering gas flow was stopped and the scattering cell allowed to evacuate. Prior to concluding the test, the photon counter background count, the metastable beam intensity, the final scattering cell pressure and the room and nozzle temperatures were recorded. The beam gas was shut off and the beam gas and scattering gas inlet manifolds were evacuated.

The metastable beam energy was varied by changing the nozzle temperature and the above procedure was repeated for each new beam energy. The average relative translational energy was calculated using the following equation for a monoenergetic beam colliding with a scattering gas that is described by a Boltzmann distribution of velocities:[17]

$$\langle E_{rel} \rangle = \frac{m \quad (Mv_0^2 + 3kT)}{2(m + M)} \tag{8}$$

where m = mass of the beam gas

M = mass of the scattering gas

$$v_0 = \underset{(perfect\ no_2)}{\text{beam velocity}} = \frac{(5kT_{no_2})^{1/2}}{(M)^{1/2}} \qquad (9)$$

T = temperature of the scattering gas

In order to obtain higher translational energies, the beam gas was seeded with hydrogen. The beam gas velocity was determined by use of a time of flight analysis outlined below, and the value inserted into equation (8).

B. TIME OF FLIGHT

The addition of hydrogen to the beam gas meant that equation (9) could not be used to calculate velocity. As mentioned earlier, a pulsed metastable beam was generated through the use of a pulse generator. A 5 μsec square wave pulse, with a frequency of 960 Hz, was delivered to a power amplifier supplying +150 V to the grid. The output from the power amplifier and the metastable beam pulse (as measured by a channeltron detector) were monitored simultaneously on an oscilloscope. A sample tracing from the oscilloscope can be seen in Figure 4. It would seem to be a simple matter to count the number of divisions between the amplifier pulse and the metastable beam peak, and divide the distance traveled by the beam, by the resulting time. This would yield the assumed beam velocity. This, however, would lead to incorrect results, due to the design of the beam excitation region. Since the beam is excited over a 2.5 cm length and there is a delay in the

FIGURE 4. Time of flight oscilloscope output. The dashed line represents the grid pulse signal.

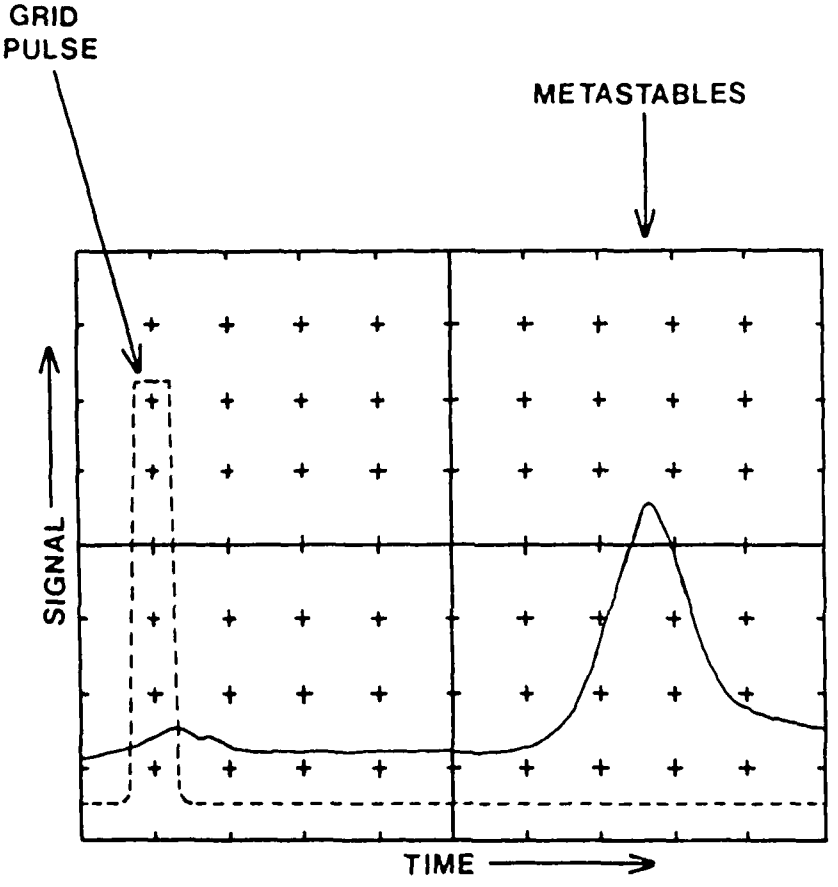
GRID
PULSE
METASTABLES
SIGNAL
TIME

transmission of the voltage pulse to the grid, it is difficult to determine the exact path length. In measurable terms, this results in a delay time between the actual beam excitation and the pulse to the grid. In order to determine the path length, measurements were made of the time between grid excitation and the arrival of unseeded metastable atoms at the detector, as a function of nozzle temperature. For each temperature, a thermal velocity was calculated and used to generate the time of flight (TOF) of the metastable beam for various assumed path lengths. The difference between these times of flight and the time between grid excitation and metastable beam arrival at the detector were tabulated, producing tables of delay times. The delay times for each path length, obtained from each nozzle temperature, were averaged and a relative error (mean value divided by the standard deviation) was calculated for each path length. The path lengths with the smallest relative errors, represent the most probable path lengths, which were then averaged to determine a mean path length and a mean delay time (the mean delay time is subtracted from the time of flight data measured on the oscilloscope). The results of this procedure were a path length of 14.45 cm and a delay time of 10.66 ± .86 μsec. These values were used in the subsequent seeded beam experiments to calculate beam velocities, which were then fed into equation (8) (Chantry equation) resulting in the

determination of the relative kinetic energy of the beam. It is of interest to note that an upper limit for the delay time of 20 μsec was determined as the result of a breakdown of an electrical cable connected to the deflector plates. This failure allowed Ar^* ions to impinge on the metastable detector and created a large ion peak on the oscilloscope. Normally, this ion peak was small and broad, making it difficult to extract any information.

C. ELASTIC SCATTERING TESTS

The purpose of this project is to measure the quenching cross section of the reaction between Ar^* and water. In these experiments we are actually measuring the total cross section for the reaction. The total cross section is a function of the quenching cross section (σ_Q) and the elastic scattering cross section ($\sigma_{elastic}$), and has a functional form of

$$\sigma_{tot} = \sigma_Q + \alpha\sigma_{elastic} \tag{10}$$

where α is a geometry factor which is a function of the entrance slit width (beam width).

The purpose of the elastic scattering test was to determine if the elastic scattering cross section was a significant fraction of the total cross section, and if we are justified in interpreting our results as representing the quenching cross section.

In order to determine if there was any significant change in the cross section, data was collected using three

different entrance slit widths (3mm, 2mm and 1mm) for a single beam energy. The observed beam length was kept constant, at 2 mm. If elastic scattering had been observed, the pressure at which the maximum observed intensity occurred, would have shifted to a lower pressure (i.e., the curves would peak at larger cross sections) as the slit width was decreased. The results of the experiment showed that the pressure at the maximum intensity remained constant, within experimental error.

Since σ_{tot} did not change significantly with slit width, $\sigma_0 >> \alpha\sigma_{elastic}$ and therefore $\sigma_{tot} \approx \sigma_0$. Thus, we are actually measuring the quenching cross section for the above reaction.

IV. DATA ANALYSIS AND RESULTS

As stated earlier, the procedure for gathering data consisted of measuring the intensity of the $OH(A^2\Sigma^+ \rightarrow X^2\Pi_i)$ emission at various scattering gas pressures for a specific beam energy (or velocity). The average background light intensity was subtracted from the measured intensity and the difference was plotted versus the scattering gas pressure. A smooth curve was then drawn through the data, with the peak of the curve denoting the point of maximum intensity. In order to increase the confidence in the point picked as the peak, the data were fit to the functional form:

$$I = A\, P_{H2O}\, \exp(-kP_{H2O}) \tag{11}$$

where

$$k = \frac{1}{P_{H2O}^{max}} \qquad \text{at } I_{max} \tag{12}$$

Given the values of I_{max} and P_{H2O}^{max} obtained earlier, the normalization constant A was calculated, as was k. These values were substituted into equation (11) and data was generated and plotted against the original experimental curve. The values of P_{H2O}^{max} and I_{max} which gave the best overlap of the experimental data were then assumed to be the best values for that metastable beam energy. An example of this type of plot is shown in Figure 5. It should be noted that Dickson and Zare[13] ascribed meaning to each term in equation (11). The linear, pressure term, is

FIGURE 5. Plot of intensity of $OH(A^2\Sigma^+ \rightarrow X^2\Pi_i)$ vs. scattering gas pressure for $\langle E_{rel} \rangle = 0.0463$ eV. Solid circles represent the experimental data. Crosses represent the data generated from equation (11) for values of I_{max} and $P_{H_2O}^{max}$ obtained from a smooth curve drawn through the experimental data.

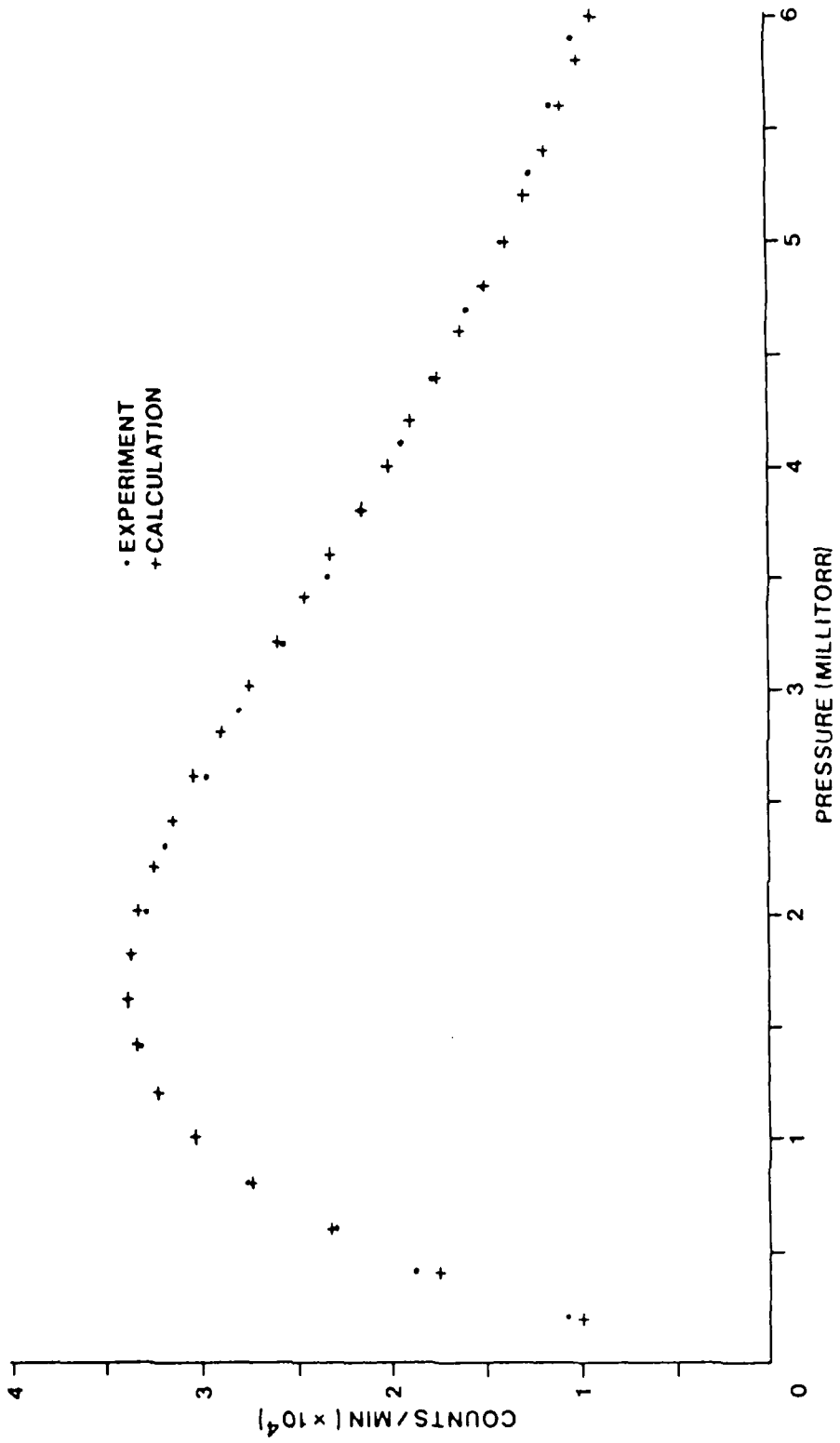
· EXPERIMENT
+ CALCULATION
COUNTS / MIN (× 10⁴)
PRESSURE (MILLITORR)
0
1
2
3
4
5
6

said to describe the formation of excited state molecules, while the exponential term describes the attenuation of the beam by the scattering gas. The term k, in equation (11) is similar to their term α (the attenuation parameter), which they relate to the total phenomenological cross section for beam removal.

Equation (11) generally predicts lower values of intensity for that part of the experimental data after the peak of the curve. This is interesting, since one would expect the opposite to take place due to collisional deactivation of OH^* with H_2O at high scattering gas pressures. The reason for the deviation from the expected results is difficult to assess since the zero of pressure is only known to ±0.05 millitorr.

The value obtained for $P_{H_2O}^{max}$ was substituted into equation (7) to obtain the value of the scattering gas number density (n_{sc}). This was then used to find the quenching cross section for the reaction at a particular energy from equation (6). The above procedure was repeated for successive beam energies and plotted as shown in Figure 6. This figure clearly shows that the quenching cross section varies with energy. Figure 7 shows a plot of log σ_0 vs. log $\langle E_{rel} \rangle$. The solid line represents the least squares fit to the data, which yields a cross section energy dependence of $E^{-0.83}$ (the correlation coefficient for the fit was calculated to be r = -0.979).

In addition to finding P_{H2O}^{max} by plotting the data as described above, it was also calculated by doing a least squares curve fit of ln(I/n) vs n for each test run. This was done as a check of the reasonableness of the value of P_{H2O}^{max} determined by the above method. In this case, n is the scattering gas number density as defined by equation (7). The slope of this plot is equal to $1/n_{max}$. By plugging the value of n_{max} into equation (7), we are able to find P_{H2O}^{max} for each test case. Table I lists P_{H2O}^{max} determined by both methods as a function of $\langle E_{rel} \rangle$, as well as the quenching cross sections.

The value of x in equation (6), which corresponds to the distance from the entrance of the scattering cell to the position where the reaction cross section was measured in the cell, was determined to be 1.1 ± 0.1 cm for data taken between 2 February 1986 and 8 July 1986. The data taken prior to 2 February 1986 was collected with the focusing lens 0.18 cm downstream of its location for the data taken between 2 February 1986 and 8 July 1986. This yields a value for x of 1.28 cm for the older data. The reason for the change in distance is a result of changing the position of the focusing lens, located between the scattering cell and the monochromator entrance slits. This was done to achieve an optimal observed emission intensity from the scattering cell.

Three tests using D_2O (obtained from Cambridge Isotope

FIGURE 6. Plot of the quenching cross section (σ_Q) vs. relative energy ($\langle E_{rel} \rangle$) for the system $Ar^* + H_2O$. Boxes indicate $Ar^* + D_2O$ cross sections.

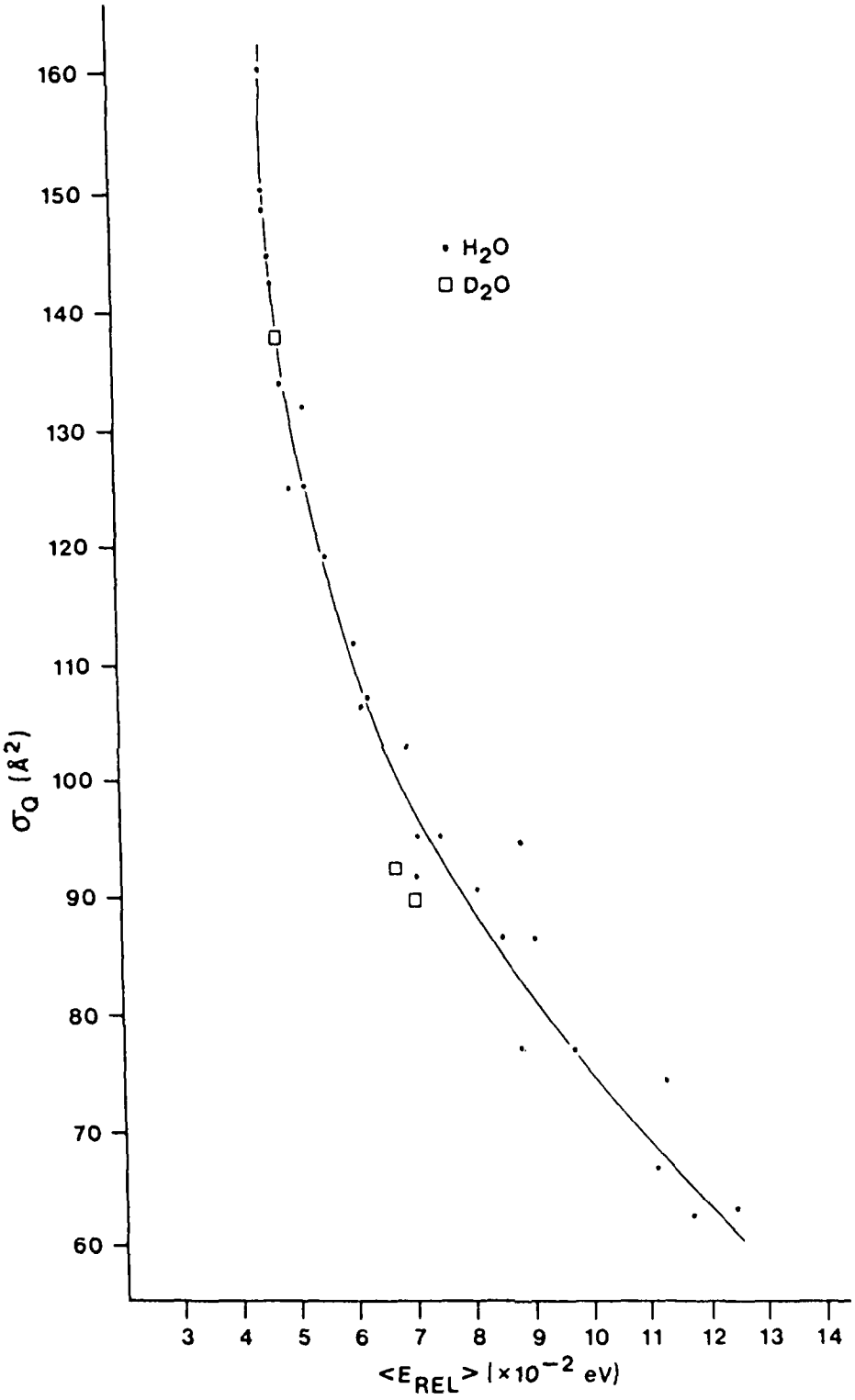
160
150
140
130
120
110
100
90
80
70
60
σ_Q (Å^2)
• H_2O
□ D_2O
3
4
5
6
7
8
9
10
11
12
13
14
<E_{REL}> (×10^{-2} eV)

FIGURE 7. Plot of log σ_0 vs. log $\langle E_{rel} \rangle$. The solid line represents the least squares curve fit to the data. In this case, log σ_0 = $-0.83 \log \langle E_{rel} \rangle + 1.04$, $r = -0.979$.

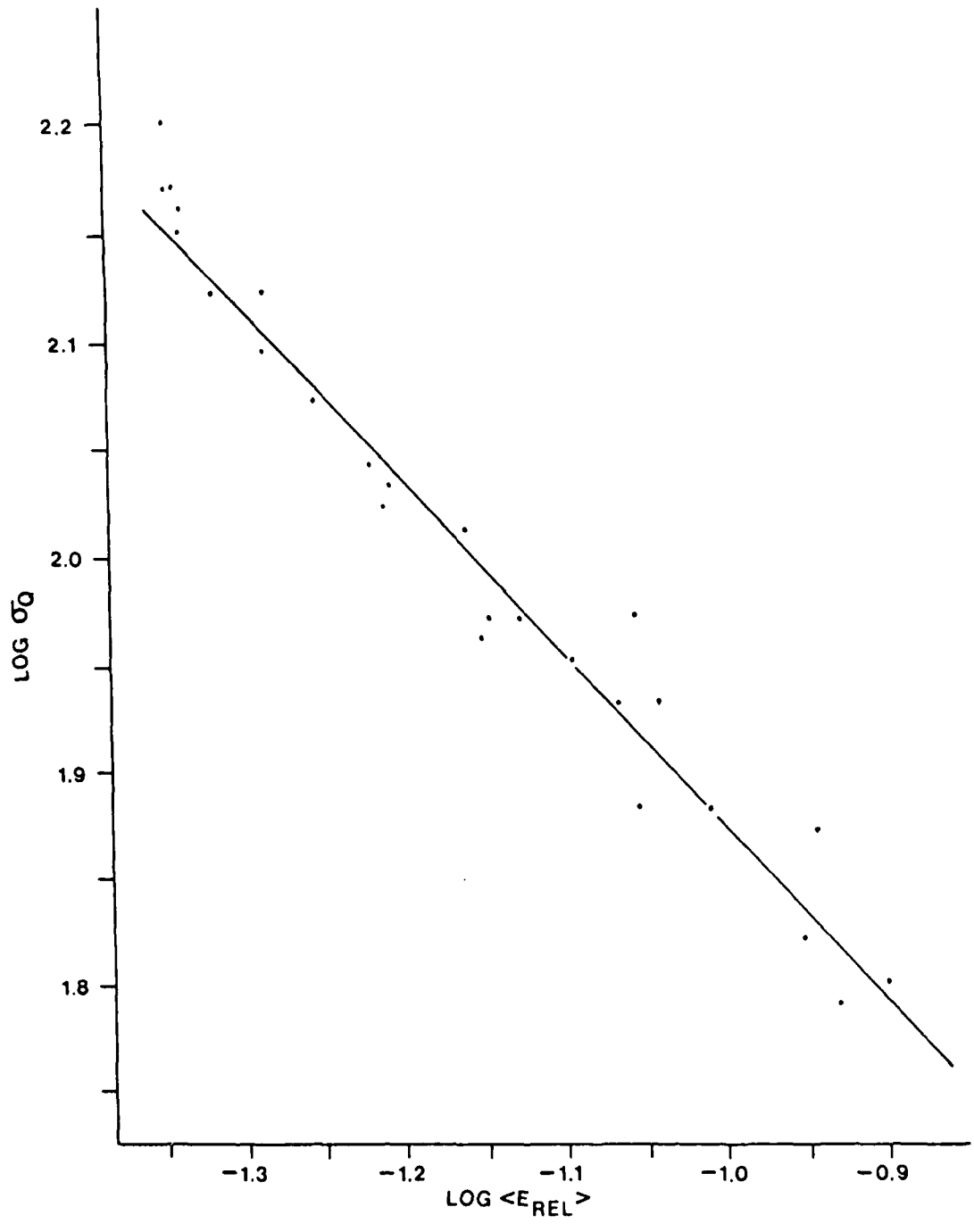
2.2
2.1
2.0
1.9
1.8
LOG σ_0
−1.3
−1.2
−1.1
−1.0
−0.9
LOG $\langle E_{REL} \rangle$

TABLE I

Comparison of $P_{H_2O}^{max}$ Values

$\langle E_{rel} \rangle$ x 10^{-2} eV	P_{max} Grap x 10^{-3} Torr	P_{max} Calc x 10^{-3} Torr	σ_0 Grap A^2	σ_0 Calc A^2
4.54	1.88	1.95	147.32	142.03
4.54	1.50	1.64	159.10	145.52
4.57	1.85	1.88	149.15	146.77
4.63	1.67	1.67	143.54	143.54
4.64	1.70	1.77	141.19	135.61
4.81	2.08	2.14	132.66	128.94
4.92	1.94	1.59	123.73	150.96
5.18	1.94	2.00	123.94	120.22
5.19	2.12	2.19	130.37	126.21
5.57	2.04	2.04	117.78	117.78
6.11	2.28	2.25	105.38	106.79
6.20	2.60	2.58	106.12	106.95
6.87	2.36	2.53	101.81	94.97
7.00	3.05	3.00	90.90	92.41
7.41	2.56	2.75	94.30	87.78
8.02	2.68	2.80	89.65	85.81
8.47	3.22	3.30	85.69	83.61
9.00	2.80	2.97	85.81	80.90
		Time of Flight Data		
6.02	2.50	2.66	110.79	104.13
7.09	2.94	2.94	94.20	94.20
8.71	3.60	4.00	76.50	68.85

TABLE I (continued)

$\langle E_{rel} \rangle$ x 10^{-2} eV	P_{max} Grap x 10^{-3} Torr	P_{max} Calc x 10^{-3} Torr	σ_0 Grap A^2	σ_0 Calc A^2
8.75	2.96	2.92	93.57	94.85
9.63	3.60	3.82	76.50	72.10
11.03	4.20	4.02	66.43	69.41
11.28	3.75	3.80	73.72	72.75
11.58	4.48	4.70	62.28	59.37
12.34	4.44	4.48	62.85	62.29
		D_2O Data		
4.74	2.05	2.26	136.11	123.46
6.65	3.05	2.97	91.48	93.95
6.97	3.15	2.93	88.58	95.23

Lab, 99.96% D) as the scattering gas were conducted in order to determine if there was any noticeable isotope effect on the quenching cross section. The data from these tests is plotted on Figure 6 along with the data for Ar^* + H_2O. There does not appear to be any noticeable isotope effect, based on the limited number of trials conducted. However, it is easily seen that the quenching cross section for Ar^* + D_2O does vary with energy.

V. DISCUSSION

A. COMPARISON OF DATA WITH OTHER SOURCES

Several researchers have investigated the quenching cross section of metastable argon with water, and have obtained a variety of results for the thermal quenching cross section at approximately 300 K. Some examples are: 99 A^2 from Sheldon and Muschlitz[9], 67 A^2 from de Jong[18] and 61 A^2 from Bourene and Le Calve.[19] By comparison, in this study an uncorrected cross section of 141 A^2 was obtained. The differences seen in these measurements can be attributed to several factors. Bourene and Le Calve and de Jong looked at the cross section for $Ar(^3P_2)$ obtained from rate constant data (where $\sigma_Q = k_Q/\langle v \rangle$), while in this work and in Sheldon and Muschlitz the cross section for $Ar(^3P_{2,0})$ was obtained. Since the ratio of $Ar(^3P_2)$ to $Ar(^3P_0)$ is assumed to be statistical (5:1), the contribution of the $^3P_0$ species to the cross section is of some significance. In addition, the methods used for finding the quenching cross section ranged from pulsed radiolysis[19] to beam/gas experiments,[9] which introduce their own biases to the results. It is of interest to note, that the mechanism for quenching of the $^3P_2$ and $^3P_0$ states are considered to be the same.[20]

As stated previously, the results of this study show that the quenching cross section of the argon/water system has an energy dependence of $E^{-0.83}$ over the range of 0.045

to 0.125 eV. This result differs from the results obtained by Corn[11] and Parr and Martin,[10] where the dissociative excitation cross section (σ_*) was measured. Their results are shown in Figures 8 and 9. They obtained an energy dependence for the cross section of $E^{-0.60}$ and $E^{-0.34}$, respectively, over the energy range of 0.046 to 0.2 eV.

The great difference in the magnitudes of the energy dependence shown above are the result of differences in the experimental procedure used in each case. In addition, Parr and Martin did not describe any method for insuring that they had eliminated the presence of nitrogen in their sample of water. Since they did not resolve their emission spectra, it is possible that nitrogen present in their water sample interfered with the measurement of the water (0,0) bandhead. This could yield an increase in the cross section of water, and therefore a decrease in the energy dependence, since the cross section for the reaction of Ar^* and N_2 increases with energy.[10,11] Corn's data on the other hand, requires the measurement of the metastable beam intensity in order to calculate the cross section for the reaction. This can be a source of error, since there is a tendency for the metastable detector used in the experiment to report lower values of intensity with time (probably due to contamination of the detector surfaces with beam gas), therefore affecting the calculation of the cross sections.

The energy dependence of the quenching cross section

FIGURES 8 AND 9. Plots of log σ_A vs. log E for Corn and Parr and Martin. Both plots examine the energy dependence of the cross section in the linear region between 0.046 and 0.2 eV.

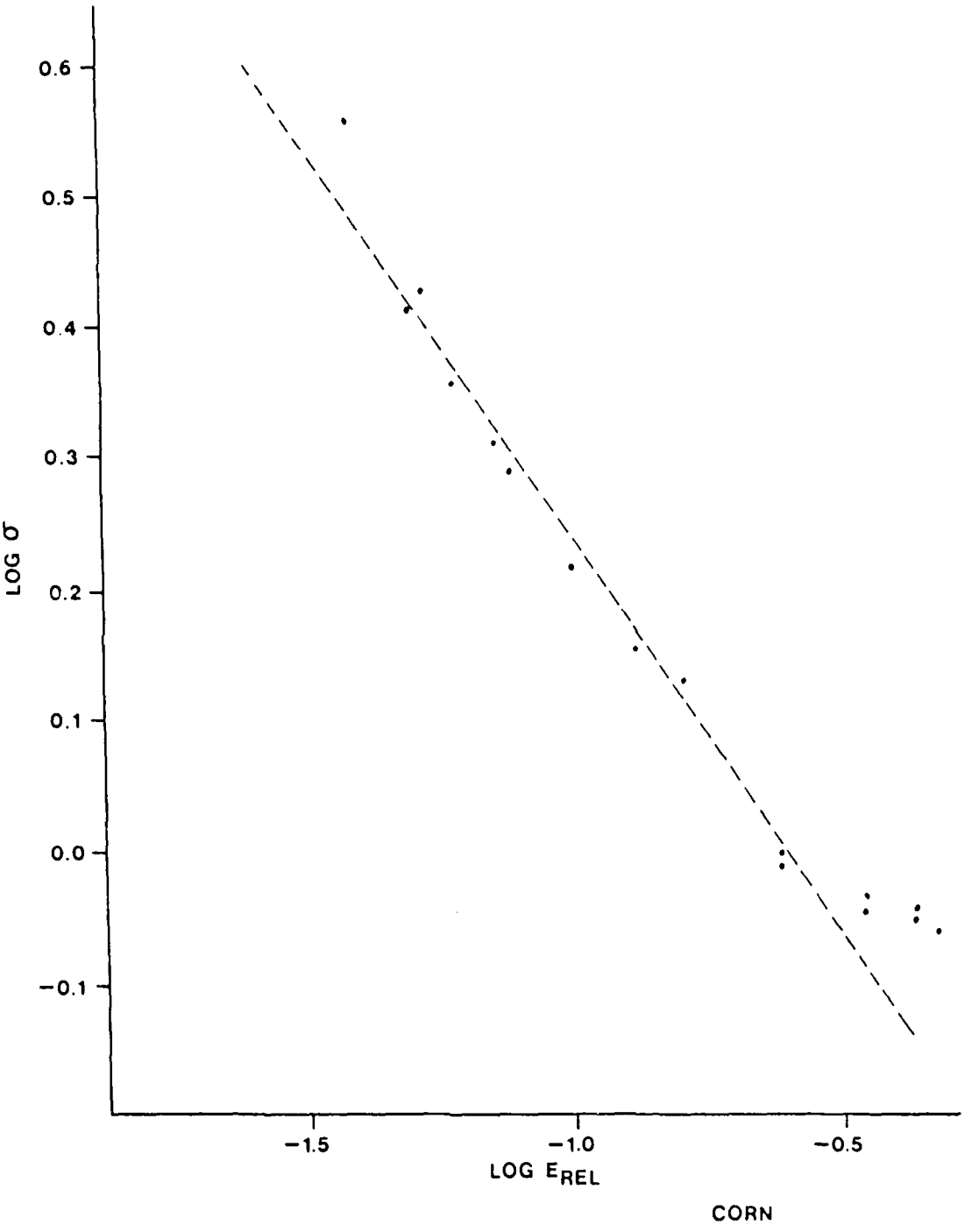
0.6
0.5
0.4
0.3
0.2
0.1
0.0
−0.1
LOG σ
−1.5
−1.0
−0.5
LOG E_{REL}
CORN

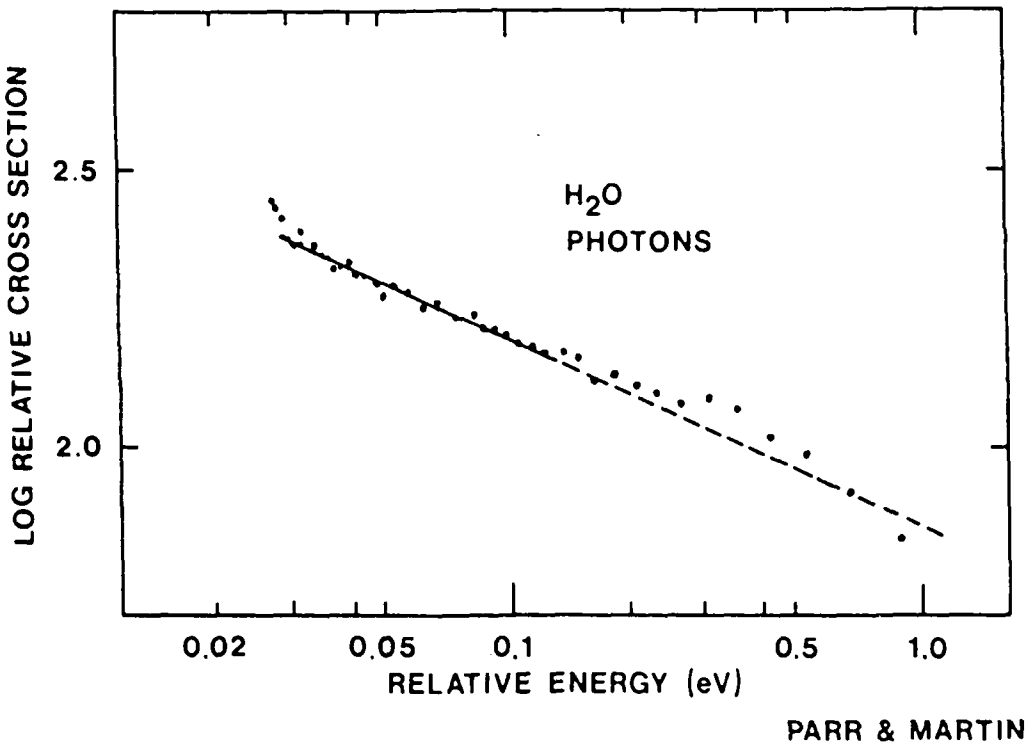
LOG RELATIVE CROSS SECTION
2.5
2.0
H_2O
PHOTONS
0.02
0.05
0.1
0.5
1.0
RELATIVE ENERGY (eV)
PARR & MARTIN

yields qualitative information on the shape of the intermolecular potential for this system. The results obtained in this work show that the cross section for the argon/water system decreases with the relative energy of the reacting species. This implies that the interaction is governed by a long range attractive potential perhaps of the form

$$V(R) \approx -C/R^6 \qquad (13)$$

where R is the distance between the center of mass of the reacting species and C is the induced-dipole-induced-dipole van der Waals coefficient for pairwise interaction.[3,21] In addition, Figure 5 shows that $\sigma_0 \dashrightarrow \infty$ as $E \dashrightarrow 0$, indicating that there is a lack of an energy barrier for the reaction of Ar^* and H_2O.[3] These results are consistent with those obtained by Corn,[11] Parr and Martin,[10] and Snyder et al.[8] Clyne[7] has suggested that the Ar^*/H_2O interaction was repulsive, while Sheldon et al.,[9] suggested that there is no energy dependence of the cross section. Clyne does not seem to justify his conclusion for a repulsive interaction, while the results of Sheldon et al., are probably an artifact of their apparatus.

In addition to the presence of long range attractive interactions, the energy dependence of the cross section also implies the presence of an attractive well in the potential.[3]

This concept of an attractive interaction has

similarities to the interaction of metastable neon and water outlined by Bentley.[22] Although the reaction of Ne^* and H_2O results in a Penning ionization process, the general interaction is probably similar to that of Ar^* and H_2O. Bentley describes a computational approach, where Ne^* attacks the oxygen portion of the water molecule along the C_{2v} axis, and proposes that an electrostatic model should be used to generate potential surfaces for this class of interacting species. The properties of neon and argon are reasonably similar, and since the reaction between Ar^* and water is governed by an attractive potential, it is likely that Ar^* approaches the water molecule along the C_{2v} axis as well. In addition, the larger polarizability of Ar^* would be expected to result in a stronger interaction between metastable argon and water.[8]

The energy transfer mechanism, and especially the dissociation mechanism for the argon-water reaction, are areas of extreme speculation. Many papers indicate that an intermediate complex $(ArHOH)^*$ is formed, followed by one or more dissociative pathways.[7,8]

B. MODELING OF THE DATA

Dr. J. Krenos, of Rutgers University, has attempted to model the data obtained in this study by two methods. The first model is simply a relationship between the cross section and the beam velocity which yields a good fit to the data. The second method is an attempt to fit the data

on the basis of realistic intermolecular interactions. The resulting equations are

$$\text{Model I} \quad \sigma = 7952 / v \tag{14}$$

$$\text{Model II} \quad \sigma = (2253 / v^{2/3})(1 - e^{-150/v}) \tag{15}$$

where v is in units of 10^3 cm/sec. Although the metastable beam exhibits a high degree of monochromaticity, a distribution of metastable atom velocities still exists. More importantly, the scattering gas velocity distribution is far from monochromatic. As a result, velocity averaging techniques were required to obtain the final model parameters. Model II, proposes the existence of a potential of the form $-C_6/R^6$ and a derived orbiting cross section,which is reduced by a curve crossing correction factor $(1 - e^{-\alpha/v})$, the factor $\alpha = 150$ gives results consistent with the experimental data. Data from these models is presented in Figure 10, along with the curve described by the experimental data.

The existence of an orbiting, attractive potential to describe the interaction of metastable argon and water has been proposed by Velasco et al.,[23] and Parr and Martin.[10] The existence of excitation transfer via curve crossing has also been suggested by Velasco[23] and Balamuta.[24] The curve crossing correction seems to fit the data reasonably well, suggesting that some of the Ar^* suffering orbiting collision is not quenched.

FIGURE 10. Plot of σ_0 vs. $\langle E_{rel} \rangle$ showing data generated from models I and II, plotted against the curve obtained from experimental data.

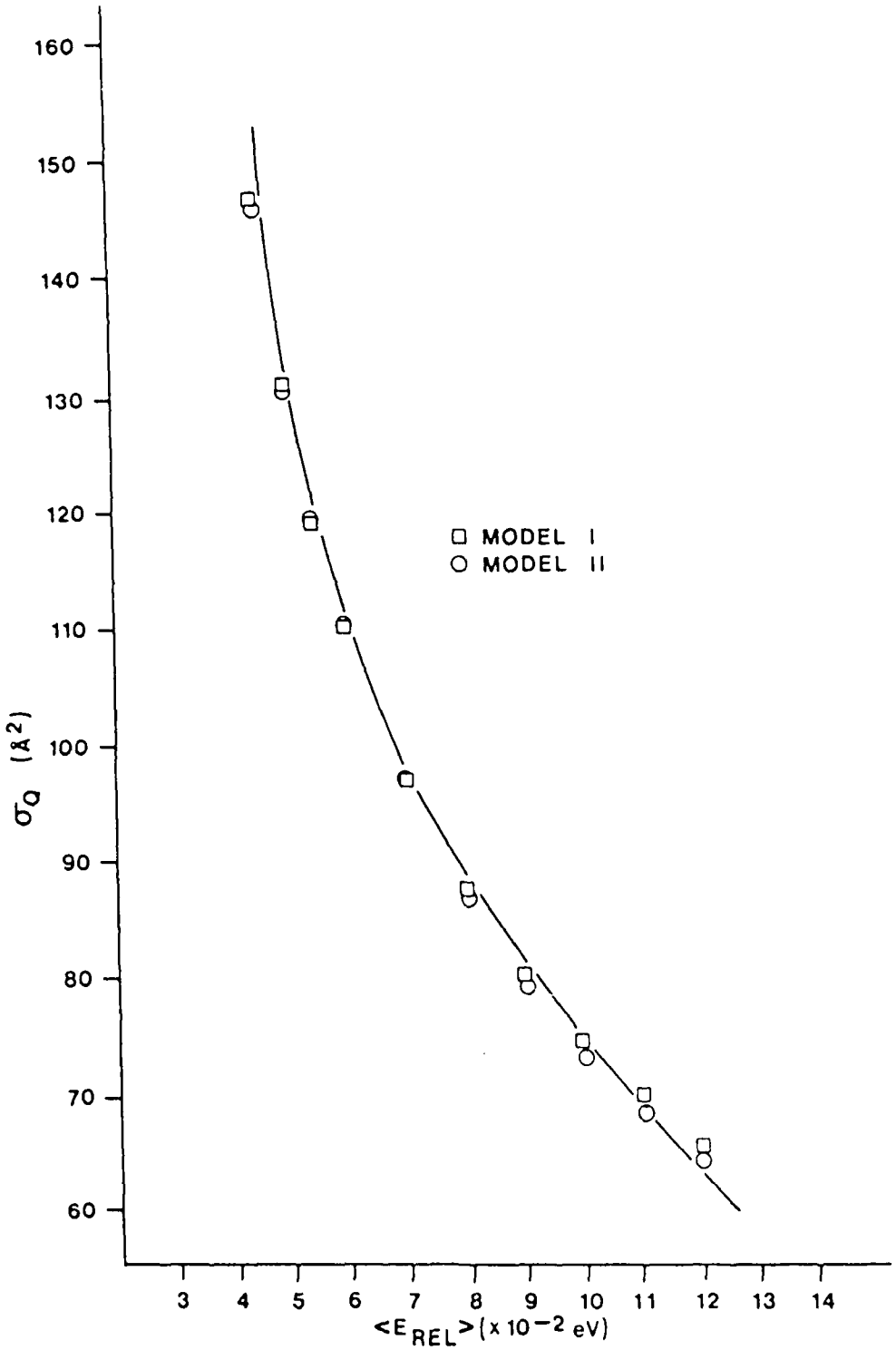
160
150
140
130
120
110
100
90
80
70
60
σ_Q (Å^2)
□ MODEL I
○ MODEL II
3
4
5
6
7
8
9
10
11
12
13
14
<E_{REL}> (x 10^{-2} eV)

C. FUTURE WORK

In order to improve the data acquisition process and gain a better understanding of the interaction processes of the Ar^* and H_2O system, several changes to the system should be accomplished. At this time, the maximum and minimum scattering gas pressures are limited by the vapor pressure of water at room temperature. As the beam energy is increased the maximum in the intensity of fluorescence vs. scattering gas pressure curve shifts to higher pressures. In order to gain information on the interaction of these species at high beam energies, higher scattering gas pressures must be achieved. In addition, in order to gain information on the low energy limit for the reaction, lower beam energies need to be achieved which requires that the nozzle be cooled. The information gained from the examination of these areas will lead to a better understanding of the potential surface which governs this system.

VI. CONCLUSION

In this work, the interaction between metastable argon atoms and ground state water molecules was investigated through the use of a molecular beam and scattering gas system. The novel approach of this investigation was the application of the procedure for the measurement of the peak intensity of the OH^* emission as a function of the scattering gas pressure to determine the quenching cross section for this reactive system. This method eliminates many of the experimental problems associated with the measurement of the total cross section for polyatomic interactions.

The uncorrected quenching cross section and the deconvoluted form were determined to vary with energy as $E^{-0.83}$ and $E^{-0.50}$, respectively. The intermolecular potential for this system was determined to be governed by long range attractive forces, with the existence of an attractive potential well.

Similarities can be seen between the metastable argon and water reaction and the interaction of metastable neon and ground state water. Since the interaction of metastable argon and water is governed by a long range attractive potential, and since argon has a large polarizability, an induced-dipole--induced-dipole interaction is probable, with metastable argon approaching the oxygen end of the water molecule along the C_{2v} axis.

This forms a metastable intermediate species, leading to a number of possible product channels.

In order to gain a better understanding of the reaction process, the energy range of the metastable beam should be expanded.

REFERENCES

1 W. C. Gardner, Jr., Rates and Mechanisms of Chemical Reactions, Benjamin/Cummings, Menlo Park, Cal., 1969.

2 R. E. Weston and H. A. Schwarz, Chemical Kinetics, Prentice Hall, Englewood Cliffs, N. J.,1972.

3 R. D. Levine and R. B. Bernstein, Molecular Reaction Dynamics, Oxford University Press, New York, N. Y., 1974, p. 173-4.

4 R. P. Wayne, Chemistry of Atmospheres, Oxford University Press, New York, N. Y., 1985, p. 88.

5 E. E. Muschlitz, Jr., Science 159, 599(1968).

6 N. E. Small-Warren and L.-Y. Chow Chin, Phys. Rev. A 11, 1777(1975).

7 M. A. A. Clyne, J. A. Coxon, D. W. Setser and D. H. Stedman, Trans. Fara. Soc. 65, 1177(1969).

8 H. L. Snyder, B. T. Smith, T. P. Parr and R. M. Martin, Chem. Phys. 65, 397(1982).

9 J. W. Sheldon and E. E. Muschlitz, Jr., J. Chem. Phys. 68, 5288(1978).

10 T. P. Parr and R. M. Martin, J. Phys. Chem. 82, 2226(1978).

11 H. D. Corn, Senior Research Paper, Rutgers University (April 1981).

12 J. Krenos, Research Proposal, Rutgers University (1985).

13 R. C. Dickson and R. N. Zare, Chem. Phys. 7, 361(1975).

14 J. R. Gordon, Y. T. Lee and D. R. Herschbach, J. Chem. Phys. 54, 2393(1971).

15 K. Bier and O. Hagena, Proc. Rarified Gas Dynamics Conference IV, II, 260(1966).

16 J. Bel Bruno, PhD Thesis, Rutgers University (1980).

17 P. J. Chantry, J. Chem. Phys. 55, 2746(1971).

18 H. J. De Jong, Chem. Phys. Letters 25, 129(1974).

19 M. Bourene and J. Le Calve, J. Chem. Phys. 58, 1452(1973).

20 K. Matsubara, Y. Oono, S. Kai and Y. Nishimura, Bulletin of the Chem. Soc. of Japan 52, 1583(1979).

21 H. L. Kramer and D. R. Herschbach, J. Chem. Phys. 53, 2792(1970).

22 J. Bentley, J. Chem. Phys. 73, 1805(1980).

23 J. E. Velasco, J. Chem. Phys. 69, 4357(1978).

24 J. Balamuta, J. Chem. Phys. 76, 2430(1982).

END

DATE

FILMED

DTIC

9-88